# Diffraction of flexural waves by finite straight cracks in an elastic sheet over water

R. Porter & D.V. Evans
School of Mathematics, University of Bristol, Bristol, BS8 1TW, UK.

May 22, 2006

**Abstract**

The diffraction of long-crested incident waves propagating within a thin flexible elastic sheet floating on water by narrow cracks is considered. The cracks are straight and each of finite length and must be parallel to one another. This arrangement lends itself to the use of Fourier transform methods, which allows the solution to a simpler problem to be used. For $N$ cracks, $2N$ coupled integral equations results for $2N$ unknown functions related to the jump in displacement and slope across each crack as a function of distance along the cracks. These integral equations are hypersingular but, in approximating their solution using Galerkin's method, a judicious choice of trial function provides maximum simplification in the algebraic equations which result.

Numerical results focus on the diffracted wave amplitudes, the maximum displacement of the elastic sheet and the stress insensity factor at the ends of the cracks. For two side-by-side cracks, large resonant motion can occur in the strip between the cracks.

## 1 Introduction

The present work is the continuation of a sequence of papers by the authors aimed at modelling the effect of cracks in large ice floes on incident flexural waves within the ice.

Early work by Press & Ewing (1951) confirmed experimentally the existence of dispersive flexural waves travelling in large sheets of ice floating on water. They developed a formula for determining the velocity of these using the coupling conditions between the ice, modelled by a thin elastic sheet, and the water beneath. Observations by Robin (1963) that large ice floes do indeed bend to allow waves to propagate through them has prompted a number of authors to consider further problems using this model and considerable progress has been made in understanding the extent of wave propagation through ice using this model despite the complexity of the governing equations. For an extensive survey article, see Squire *et al* (1995).

One of the earliest approaches can be found in Stoker (1957) who used the shallow water equations to determine the reflection and transmission of a surface gravity wave by a thin freely-floating elastic sheet of finite extent. Wave solutions in the water regions were matched at the edges of the sheet with solutions of the sixth-order ordinary differential equation governing the sheet displacement, using continuity and free edge conditions. Shortly afterwards, Evans & Davies (1968) considered the scattering of obliquely-incident water waves by a semi-infinite thin elastic sheet floating on water of finite depth, using the full linear water wave theory. They used the Wiener-Hopf method to obtain an explicit solution but the complicated fifth-order differential operator satisfied by the velocity potential on the sheet arising from the coupling of the sheet displacement and water velocity, prevented detailed numerical calculations from being made.

Further simpler models describing waves in ice continued to be developed, primarily by researchers in New Zealand, but it was the possibility of constructing massive floating runways in Japan which led to a dramatic increase in activity in the general area of VLFS (very large floating

structures) and in particular in developing good mathematical models of the bending of structures in waves. The work of Evans & Davies (1968) was revisited by a number of authors including Chung & Fox (2002), Balmforth & Craster (1999) and Tkacheva (2001), whilst numerical results were obtained for scattering by *finite* elastic sheets by Hermans (2004). An indication of the renewed interest in the field is the existence of a sequence of symposia on hydroelasticity in marine enviroments. See, for example, Eatock Taylor (2003).

Problems involving cracks in an elastic sheet floating on water have been considered by a number of authors. Cracks are clearly important in influencing the rate at which ice floes break up under wave action, and they have the added attraction of yielding to exact mathematical analysis in certain cases, in contrast to problems involving finite open water regions or finite elastic plates. The simplest such problem is the infinitely-long straight-line crack in a floating elastic sheet entirely covering the water surface. A number of authors have considered the scattering of incident flexural waves by such a crack, including Squire & Dixon (2000), Williams & Squire (2002) and the present authors (Evans & Porter (2003)) who solved the problem using full linear theory in finite water depth and obliquely-incident waves. The solution can be shown to depend upon two fundamental quantities, namely the jump in displacement and slope across the free edges of the crack. In a subsequent paper (Porter & Evans (2005)) the authors showed how the method could be extended to multiple cracks, the solution now determined by an algebraic system of $2N$ equations for quantities related to the jump in slope and displacement at each of the $N$ cracks.

In the present work we consider the more difficult and more relevant problem of the scattering of flexural waves by a finite number of straight-line cracks, each of *finite* length. The problem now no longer admits an explicit solution but requires the solution of integral equations for the unknown jumps in slope and displacement which are now functions defined along the length of the cracks.

In previous work on infinitely-long cracks in elastic plates over water the wave energy must be transmitted across the crack through the water region. No such mechanism for transmission of wave energy is available in the corresponding problem of an elastic sheet *in vacuo*. However, in the problem involving a finite length crack, as considered in this paper, there is a non-trivial equivalent problem in the simpler *in vacuo* case. Thus Andronov and Belinsky (1995), subsequently denoted by AB95, have considered precisely this problem, namely the scattering of plane incident flexural waves by a finite straight-line crack in an elastic plate of infinite extent. Despite this similarity, the presence of the water region below the sheet in the present problem allows the direct transmission of wave energy to the leeward side of the crack. For an elastic sheet *in vacuo* as considered by AB95, wave energy is transmitted to the leeward side of the crack solely by diffraction from the edges of the crack.

Advantage is taken of the ideas behind the approach of AB95 in the more complicated problem considered here, and it is remarkable how similar much of the analysis is in the single crack case. Thus their approach, like ours, is based on the use of Fourier transforms aligned with the direction of the crack. An added complication introduced here is that we consider multiple parallel cracks whilst AB95, by concentrating on a single crack were able to consider simpler symmetric and anti-symmetric components of the problem each defined in a half-plane. It is not possible to make such a decomposition in the more general problem treated here, and so there is a significant departure from the work of AB95 early on in the analysis. In this respect, the foundation of the solution presented here uses recent work of Porter & Evans (2005) who provided a solution for multiple parallel cracks of *infinite* length which, as discussed, has no analogue in the problem considered by AB95.

In section 2, we provide a statement of the linearised boundary-value problem, and discuss conditions which apply along the cracks and at infinity. In the main part in section 3, coupled integral equations are derived for functions which are related to the jumps in slope and displacement across each crack. Although the analysis is more complicated than in AB95, a vital part of this derivation is to show that the resulting integral equations are hypersingular (that is, the kernel

has a component which is two or more derivatives of a logarithm). This property is evidently a consequence of the nature of the solution at the ends of the cracks. Details of a numerical solution based upon the Galerkin procedure is presented in section 4, which again draws upon the work of AB95, especially on the resolution of the hypersingular nature of the integral operators. In sections 5 and 6, respectively, expressions for the far-field diffraction coefficients and stress intensity factors are derived. The latter quantities are of particular interest, as they provide a measure of the likelihood that dynamic fracture occurs in the elastic sheet. Results are presented and discussed in section 7 and the paper is concluded in section 8, where further generalisations to the present work are considered.

## 2 Formulation of the problem

A flexural-gravity wave propagates from infinity within an isotropic elastic plate of constant thickness $d$ and density $\rho_p$, with Young's modulus $E$ and Poisson's ratio $\nu$. The wave propagates with wavelength $\lambda$ at an angle $\theta_{inc}$ with respect to the positive $x$ axis, where $(x, y, z)$ are cartesian coordinates with $z$ measured vertically upwards and $z = 0$ coinciding with the lower surface of the undisturbed plate. The plate rests on a fluid of density $\rho_w$ and constant depth $h$. The elastic plate contains an arbitrary number of narrow straight cracks each of finite length which diffract the incident wave. The cracks are parallel to one another and occupy the set $L = \cup_{i=1}^{N} L_i$ where $L_i = \{x = c_i,\ a_i^- < y < a_i^+\}$ for $i = 1, \ldots, N$.

When in motion, the lower surface of the plate is described by $z = \zeta(x, y, t)$ where $t$ represents time. Under the usual assumptions of linearised theory, that the fluid is inviscid and incompressible and that the flow is irrotational and undergoes small amplitude motions, there exists a velocity $\Phi(x, y, z, t)$ such that

$$\nabla^2 \Phi = 0, \qquad \text{in the fluid} \tag{2.1}$$

where $\nabla = (\partial/\partial x, \partial/\partial y, \partial/\partial z)$ with $\Phi_z = 0$ on $z = -h$. Within the fluid, the linearised version of Bernoulli's equation for the pressure $p(x, y, z)$ is

$$p = p_a + \rho_p g d - \rho_w \Phi_t - \rho_w g z, \qquad -h < z < \zeta \tag{2.2}$$

where $g$ is gravitional acceleration and $p_a$ is constant atmospheric pressure.

The motion of the plate is described using thin plate, or Kirchhoff, theory in which plate properties are averaged across the thickness of the plate and is due to the difference in pressure across it, so that (Timoshenko & Woinowsky-Krieger (1959))

$$p|_{z=\zeta} = p_a + \rho_p g d + D\nabla_h^4 \zeta + \rho_p d \zeta_{tt} \tag{2.3}$$

where $D = Ed^3/(12(1 - \nu^2))$ is the flexural rigidity of the elastic plate and $\nabla_h = (\partial/\partial x, \partial/\partial y)$. Combining (2.2) on $z = \zeta$ with (2.3) and linearising about $z = 0$ gives

$$D\nabla_h^4 \zeta + \rho_p d \zeta_{tt} + \rho_w \Phi_t + \rho_w g \zeta = 0, \qquad \text{on } z = 0. \tag{2.4}$$

The kinematic condition, linearised about $z = 0$ provides additional coupling between the fluid and the plate with

$$\zeta_t = \Phi_z, \qquad \text{on } z = 0. \tag{2.5}$$

The assumption of a time harmonic motion of angular frequency $\omega$ so that $\Phi(x, y, z, t) = \Re\{-\mathrm{i}\omega\phi(x, y, z)\mathrm{e}^{-\mathrm{i}\omega t}\}$ and $\zeta(x, y, t) = \Re\{\eta(x, y)\mathrm{e}^{-\mathrm{i}\omega t}\}$ reduces (2.4) and (2.5) to

$$(\mathcal{L}\phi)(x, y) \equiv (\beta\nabla_h^4 + 1 - \delta)\eta - \kappa\phi|_{z=0} = 0 \tag{2.6}$$

where

$$\eta = \phi_z|_{z=0} \tag{2.7}$$

and $\beta = D/\rho_w g$, $\delta = (\rho_p/\rho_w)\kappa d$ and $\kappa = \omega^2/g$, whilst

$$\nabla^2\phi = 0, \qquad -h < z < 0 \tag{2.8}$$

and

$$\phi_z = 0, \qquad \text{on } z = -h. \tag{2.9}$$

Equations (2.6) and (2.7) hold wherever $\eta$ is continuous which excludes the cracks where the boundary conditions are enforced to ensure vanishing of bending moments and shearing stresses. These are given by (Timoshenko & Woinowsky-Krieger (1959))

$$\left.\begin{aligned}(\mathcal{B}\eta)(x,y) &\equiv \eta_{xx} + \nu\eta_{yy} \to 0,\\ (\mathcal{S}\eta)(x,y) &\equiv \eta_{xxx} + \nu_1\eta_{xyy} \to 0,\end{aligned}\right\} \qquad x \to c_i^{\pm},\ a_i^- < y < a_i^+ \tag{2.10}$$

where $\nu_1 = 2 - \nu$. The functions $(\mathcal{B}\eta)(x,y)$ and $(\mathcal{S}\eta)(x,y)$ are continuous away from the cracks and, on account of (2.10), are therefore continuous for all $x, y$ in the plane. In particular, we note the jump conditions

$$[(\mathcal{B}\eta)]_i = [(\mathcal{S}\eta)]_i = 0, \qquad -\infty < y < \infty \tag{2.11}$$

which will be needed later, where we have introduced the notation

$$[u]_i = \lim_{x\to c_i^+}\{u(x,y)\} - \lim_{x\to c_i^-}\{u(x,y)\}.$$

There are further conditions that apply at the ends of the cracks. Thus from AB95 or Norris & Wang (1994) it is known that

$$[\eta]_i \sim (\pm(a_i^{\pm} - y))^{3/2} \qquad \text{and} \qquad [\eta_x]_i \sim (\pm(a_i^{\pm} - y))^{1/2}, \qquad \text{as } y \to a_i^{\pm} \tag{2.12}$$

the limit being taken from within the crack.

The incident wave, which propagates in the direction $\theta_{inc}$ with respect to the positive $x$-axis is defined by

$$\phi_0(x,y,z) = \mathrm{e}^{\mathrm{i}m_0 x}\mathrm{e}^{\mathrm{i}l_0 y}Y_0(z)$$

with corresponding plate elevation

$$\eta_0(x,y) = \mathrm{e}^{\mathrm{i}m_0 x}\mathrm{e}^{\mathrm{i}l_0 y}Y_0'(0) \tag{2.13}$$

where $Y_0(z) = \cosh\gamma_0(z+h)$ and

$$m_0 = \gamma_0\cos\theta_{inc} \qquad \text{and} \qquad l_0 = \gamma_0\sin\theta_{inc}. \tag{2.14}$$

Here, $\gamma_0 = 2\pi/\lambda$ is the wavenumber of the incident wave and is determined as the unique positive root of the dispersion relation

$$K(\gamma) \equiv (\beta\gamma^4 + 1 - \delta)\gamma\sinh\gamma h - \kappa\cosh\gamma h = 0 \tag{2.15}$$

In addition to $\gamma_0$, there are four (generally) complex roots $\gamma = \pm p \pm \mathrm{i}q$, where $p, q > 0$, the two having positive imaginary parts being labelled $\gamma_{-1} = p + \mathrm{i}q$ and $\gamma_{-2} = -p + \mathrm{i}q$ and an infinite sequence of pure imaginary roots, $\pm\gamma_n$, $n = 1, 2, \ldots$ arranged such that $0 < \Im\{\gamma_n\} < \Im\{\gamma_{n+1}\}$. The distribution of the roots is described in Evans & Davies (1968) or Squire *et al* (1995). For certain (unphysical) parameters the four complex roots may all become pure imaginary. A detailed analysis is given by Williams (2005).

The relation (2.15) is derived by separating variables for a plate with no cracks which yields solutions of the form

$$\mathrm{e}^{\pm\mathrm{i}\gamma_n x}Y_n(z) \qquad \text{where} \qquad Y_n(z) = \cosh\gamma_n(z+h) \tag{2.16}$$

assuming, without loss of generality, no variation in the $y$-direction.

The diffracted part of the wave field satisfies the Sommerfeld radiation condition,

$$r^{1/2}(u_r - i\gamma_0 u) \to 0, \qquad \text{as } r = (x^2+y^2)^{1/2} \to \infty \tag{2.17}$$

for both $u = \eta_d \equiv \eta - \eta_0$ and $u = \phi_d \equiv \phi - \phi_0$, the latter holding for each fixed depth in $z \in [-h, 0]$.

## 3 Derivation of integral equations

We introduce the Fourier transforms

$$\bar{\phi}(x,l,z) = \int_{-\infty}^{\infty} \phi(x,y,z)\mathrm{e}^{-\mathrm{i}ly}dy \tag{3.1}$$

with inverse

$$\phi(x,y,z) = \frac{1}{2\pi}\int_{-\infty}^{\infty} \bar{\phi}(x,l,z)\mathrm{e}^{\mathrm{i}ly}dl.$$

and

$$\tilde{\phi}(k,l,z) = \int_{-\infty}^{\infty} (\bar{\phi}(x,l,z) - \bar{\phi}_0(x,l,z))\mathrm{e}^{-\mathrm{i}kx}dx \tag{3.2}$$

with inverse

$$\bar{\phi}(x,l,z) = \bar{\phi}_0(x,l,z) + \frac{1}{2\pi}\int_{-\infty}^{\infty} \tilde{\phi}(k,l,z)\mathrm{e}^{\mathrm{i}kx}dk.$$

where $\bar{\phi}_0$ is the transform in $y$ of the incident wave potential and we are not concerned with evaluating this in what follows. Functions and operators with bars or tildes will henceforth denote that they have been transformed according to (3.1) and (3.2).

Taking transforms in $y$ in (2.6)–(2.9) gives

$$\bar{\phi}_{xx} + \bar{\phi}_{zz} - l^2\bar{\phi} = 0, \qquad -h < z < 0, \ \ -\infty < x < \infty$$

with

$$\bar{\phi}_z = 0, \qquad \text{on } z = -h$$

and

$$(\bar{\mathcal{L}}\bar{\phi})(x,l) = \left(\beta\left(\frac{\partial^2}{\partial x^2} - l^2\right)^2 + 1 - \delta\right)\bar{\eta} - \kappa\bar{\phi}|_{z=0} = 0, \qquad -\infty < x < \infty \tag{3.3}$$

where

$$\bar{\eta} = \bar{\phi}_z|_{z=0}$$

Crucially in what is to follow, since (2.11) applies over *all* $y$ (on the cracks and their extensions to infinity), we preserve the jump conditions in transform space, implying that

$$[(\bar{\mathcal{B}}\bar{\eta})(x,l)]_i = [(\bar{\mathcal{S}}\bar{\eta})(x,l)]_i = 0, \qquad \text{for } -\infty < l < \infty \tag{3.4}$$

for $i = 1,\ldots,N$ where

$$(\bar{\mathcal{B}}\bar{\eta})(x,l) = \bar{\eta}'' - \nu l^2\bar{\eta}, \qquad \text{and} \qquad (\bar{\mathcal{S}}\bar{\eta})(x,l) = \bar{\eta}''' - \nu_1 l^2\bar{\eta}' \tag{3.5}$$

and where the primes denote differentiation with respect to $x$. Applying transforms in $x$ now gives

$$\tilde{\phi}_{zz} - \gamma^2\tilde{\phi} = 0, \qquad -h < z < 0$$

where $\gamma^2 = k^2 + l^2$ and $\tilde{\phi}_z = 0$ on $z = -h$ which implies that

$$\tilde{\phi}(k,l,z) = A(k,l)\cosh\gamma(z+h). \tag{3.6}$$

The steps that follow represent the crux of the method. We take a different approach to that of AB95 who used the geometric symmetry of a single crack to decompose the problem into two separate problems in which various conditions were satisfied automatically by the decomposition.

Defining $\tilde{\eta} = \tilde{\phi}_z|_{z=0}$ and applying (3.2) to (3.3) now gives

$$0 = \int_{-\infty}^{\infty} (\bar{\mathcal{L}}(\bar{\phi} - \bar{\phi}_0))(x,l)\mathrm{e}^{-\mathrm{i}kx}dx = (\beta\gamma^4 + 1 - \delta)\tilde{\eta} - \kappa\tilde{\phi}|_{z=0} + \beta I(k,l) \tag{3.7}$$

where

$$I(k,l) = \int_{-\infty}^{\infty} \left\{ \left( \left( \frac{\partial^2}{\partial x^2} - l^2 \right)^2 (\bar{\eta} - \bar{\eta}_0) \right) \; G - \left( \left( \frac{\partial^2}{\partial x^2} - l^2 \right)^2 G \right) \; (\bar{\eta} - \bar{\eta}_0) \right\} dx$$

and we have used the abbreviation $G = \mathrm{e}^{-\mathrm{i}kx}$. Notice that (3.7) has been arranged such that the second term in the integral $I$ cancels the leading term, $\beta\gamma^4\tilde{\eta}$. This leaves an integral $I$ which has a structure reminiscent of Green's identity ($G$ is introduced to highlight this connection), but which does not vanish identically on account of the discontinuous nature of the function $\bar{\eta}$ and its derivatives. Hence, the integral $I$ must be calculated by dividing the range of integration over discrete intervals which exclude the values $x = c_i$, at which $\bar{\eta}$ and its derivatives possess discontinuities, before then taking limits. This process results, after integration by parts, in

$$I(k,l) = \sum_{i=1}^{N} \left\{ [\bar{\eta}'''G - G'''\bar{\eta}]_i - [\bar{\eta}''G' - G''\bar{\eta}']_i - 2l^2[\bar{\eta}'G - G'\bar{\eta}]_i \right\}$$

where the fact that $\bar{\eta}_0$ and its derivatives in $x$ are continuous functions has been used.

The contribution from the limits as $|x| \to \infty$ in the integral have been set to zero by assuming a small negative imaginary part in the frequency which will eventually tend to zero. This has the effect of moving the real wavenumber $k_0$ into the upper-half complex plane, ensuring that $\bar{\eta} - \bar{\eta}_0$ decays exponentially as $|x| \to \infty$.

Using the transformed jump conditions (3.4) with (3.5) to eliminate $\bar{\eta}'''$ and $\bar{\eta}''$ gives

$$I(k,l) = \sum_{i=1}^{N} \left\{ (G'' - \nu l^2 G)_{x=c_i}[\bar{\eta}']_i - (G''' - \nu_1 l^2 G')_{x=c_i}[\bar{\eta}]_i \right\} \tag{3.8}$$

after some rearrangement in which the relation $\nu + \nu_1 = 2$ and the fact that $G$ and its derivatives are continuous for all $x$ are used. Using the definition of the operators $\bar{\mathcal{B}}$ and $\bar{\mathcal{S}}$ in (3.8) gives

$$I(k,l) = \sum_{i=1}^{N} \left\{ (\bar{\mathcal{B}}G)(c_i,l)\bar{P}_i(l) - (\bar{\mathcal{S}}G)(c_i,l)\bar{Q}_i(l) \right\} \tag{3.9}$$

where we have introduced the functions $\bar{P}_i(l) = [\bar{\eta}']_i$, $\bar{Q}_i(l) = [\bar{\eta}]_i$, for $i = 1, 2, \ldots, N$. Thus, $I(k,l)$ depends upon the lateral position, $c_i$ of each crack in an explicit way, but also the length of each crack implicitly through the functions $\bar{P}_i(l)$ and $\bar{Q}_i(l)$, which are the Fourier transforms of the jumps in the gradient and elevation along $x = c_i$.

We note from the definition of $G = \mathrm{e}^{-\mathrm{i}kx}$ that

$$\left.\begin{aligned} (\bar{\mathcal{B}}G)(c_i,l) &= -(k^2 + \nu l^2)\mathrm{e}^{-\mathrm{i}kc_i}, \\ (\bar{\mathcal{S}}G)(c_i,l) &= \mathrm{i}k(k^2 + \nu_1 l^2)\mathrm{e}^{-\mathrm{i}kc_i}. \end{aligned}\right\}$$

Using (3.6) in (3.7) gives

$$A(k,l) = \beta I(k,l)/K(\gamma),$$

where $K(\gamma)$ is given by (2.15) and $I(k,l)$ is given by (3.9) and so

$$\bar{\phi}(x,l,z) = \frac{\beta}{2\pi} \int_{-\infty}^{\infty} \frac{\cosh\gamma(z+h)}{K(\gamma)} I(k,l)\mathrm{e}^{\mathrm{i}kx}dk. \tag{3.10}$$

At this point it is convenient to define the related function

$$\bar{\chi}(x,l,z) = \frac{1}{2\pi}\int_{-\infty}^{\infty} \frac{\cosh\gamma(z+h)}{K(\gamma)} \mathrm{e}^{\mathrm{i}kx} dk \tag{3.11}$$

and are reminded that the small imaginary part in the frequency has moved the poles (for $l < \gamma_0$) at $k_0$ and $-k_0$ into the upper- and lower-half planes respectively, where

$$\gamma_n^2 = k_n^2 + l^2, \qquad n = -2, -1, 0, 1, \ldots$$

and $\gamma_n$ are the zeros of $K(\gamma)$, as defined by (2.14). By deforming the contour of integration into the upper-half plane for $x > 0$ and into the lower-half plane for $x < 0$, the integral in (3.11) can be expressed as an infinite series, thus

$$\bar{\chi}(x,l,z) = \mathrm{i}\sum_{n=-2}^{\infty} \frac{Y_n'(0)Y_n(z)}{2k_nC_n} \mathrm{e}^{\mathrm{i}k_n|x|}$$

where $C_n = \frac{1}{2}(\kappa h + (5\beta\gamma_n^4 + 1 - \delta)(Y_n'(0))^2)$ and $Y_n(z)$ are the depth eigenfunctions defined by (2.16). In this derivation, we have used the relation $K'(\gamma_n) = -K'(-\gamma_n) = 2k_nC_n/Y_n'(0)$.

It can be noticed that the function $\chi$ which gives rise to $\bar{\chi}$ in (3.11) represents a fundamental point source on the elastic-plate loaded free surface.

It is now straightforward to show, by taking (3.10) with (3.9), that

$$\bar{\phi}(x,l,z) = \bar{\phi}_0(x,l,z) + \sum_{i=1}^{N} \left\{\bar{\psi}_s(x-c_i,l,z)\bar{P}_i(l) + \bar{\psi}_a(x-c_i,l,z)\bar{Q}_i(l)\right\}$$

where we have defined

$$\bar{\psi}_s(x,l,z) = \beta(\bar{\mathcal{B}}\bar{\chi})(x,l,z) \qquad \text{and} \qquad \bar{\psi}_a(x,l,z) = -\beta(\bar{\mathcal{S}}\bar{\chi})(x,l,z).$$

In terms of infinite series, we have

$$\bar{\psi}_s(x,l,z) = \mathrm{i}\beta\sum_{n=-2}^{\infty} \frac{g_nY_n'(0)}{2k_nC_n} Y_n(z)\mathrm{e}^{\mathrm{i}k_n|x|}$$

and

$$\bar{\psi}_a(x,l,z) = -\mathrm{i}\beta\,\mathrm{sgn}(x)\sum_{n=-2}^{\infty} \frac{h_nY_n'(0)}{2k_nC_n} Y_n(z)\mathrm{e}^{\mathrm{i}k_n|x|}$$

where $\mathrm{sgn}(x)$ is the signum function and

$$g_n = -(\nu l^2 + k_n^2), \qquad \text{and} \qquad h_n = -\mathrm{i}k_n(\nu_1 l^2 + k_n^2).$$

The suffices $s$ and $a$ have been chosen since it can easily be seen that the functions $\bar{\psi}_s$ and $\bar{\psi}_a$ are symmetric and antisymmetric (respectively) about $x = 0$.

We are now in a position to make the inverse transform in $y$. Thus

$$\phi(x,y,z) = \phi_0(x,y,z) + \frac{1}{2\pi}\sum_{i=1}^{N}\int_{-\infty}^{\infty} \left\{\bar{\psi}_s(x-c_i,l,z)\bar{P}_i(l) + \bar{\psi}_a(x-c_i,l,z)\bar{Q}_i(l)\right\}\mathrm{e}^{\mathrm{i}ly} dl. \tag{3.12}$$

Integral equations for the functions $P_i(t)$ and $Q_i(t)$, $i = 1, 2, \ldots, N$ are now obtained by applying the free edge conditions (2.10) before using convolution to invert the transform. Since the expression

for $\phi(x,y,z)$ in (3.12) has the jump conditions (2.11) already incorporated, these edge conditions need only be applied from one of the two sides. Thus, we have

$$-(\mathcal{B}\eta_0)(c_j,y) = \frac{1}{2\pi}\sum_{i=1}^{N}\int_{-\infty}^{\infty}\left\{\bar{P}_i(l)\bar{K}_s(d_{ji},l) + \bar{Q}_i(l)\bar{K}_a(d_{ji},l)\right\}\mathrm{e}^{\mathrm{i}ly}dl, \qquad y\in(a_j^-,a_j^+) \tag{3.13}$$

where $d_{ji} = c_j - c_i$ and

$$\left.\begin{aligned}\bar{K}_s(d_{ji},l) &= (\bar{\mathcal{B}}\bar{w}_s)(d_{ji},l) = \mathrm{i}\beta\sum_{n=-2}^{\infty}\frac{g_n^2(Y_n'(0))^2}{2k_nC_n}\mathrm{e}^{\mathrm{i}k_n|d_{ji}|}\\ \bar{K}_a(d_{ji},l) &= (\bar{\mathcal{B}}\bar{w}_a)(d_{ji},l) = -\mathrm{i}\beta\mathrm{sgn}(d_{ji})\sum_{n=-2}^{\infty}\frac{g_nh_n(Y_n'(0))^2}{2k_nC_n}\mathrm{e}^{\mathrm{i}k_n|d_{ji}|}\end{aligned}\right\} \tag{3.14}$$

and we have written $\bar{w}_{s,a}(x,l) = \partial\bar{\psi}_{s,a}/\partial z|_{z=0}$. Application of the zero-stress condition similarly gives

$$-(\mathcal{S}\eta_0)(c_j,y) = \frac{1}{2\pi}\sum_{i=1}^{N}\int_{-\infty}^{\infty}\left\{\bar{P}_i(l)\bar{L}_s(d_{ji},l) + \bar{Q}_i(l)\bar{L}_a(d_{ji},l)\right\}\mathrm{e}^{\mathrm{i}ly}dl, \qquad y\in(a_j^-,a_j^+) \tag{3.15}$$

where

$$\left.\begin{aligned}\bar{L}_s(d_{ji},l) &= (\bar{\mathcal{S}}\bar{w}_s)(d_{ji},l) = \mathrm{i}\beta\mathrm{sgn}(d_{ji})\sum_{n=-2}^{\infty}\frac{g_nh_n(Y_n'(0))^2}{2k_nC_n}\mathrm{e}^{\mathrm{i}k_n|d_{ji}|},\\ \bar{L}_a(d_{ji},l) &= (\bar{\mathcal{S}}\bar{w}_a)(d_{ji},l) = -\mathrm{i}\beta\sum_{n=-2}^{\infty}\frac{h_n^2(Y_n'(0))^2}{2k_nC_n}\mathrm{e}^{\mathrm{i}k_n|d_{ji}|}.\end{aligned}\right\} \tag{3.16}$$

The case of $d_{ji}=0$ will be treated shortly. At this point we remark that equations (3.13) and (3.15) represent integral equations for the functions $\bar{P}_i(l)$, $\bar{Q}_i(l)$ for $-\infty<l<\infty$. However, these integral equations are not in a particularly suitable form for computation. In particular, the behaviour of the unknown functions $\bar{P}_i(l)$, $\bar{Q}_i(l)$ for large $|l|$ are not known at this stage.

Instead, we will derive an alternative set of integral equations which are more amenable to numerical methods. In order to do so, we need to analyse the convergence of the series which define $\bar{K}_{s,a}(d_{ji},l)$ and $\bar{L}_{s,a}(d_{ji},l)$ and their behaviour for large $|l|$ which is required to interpret the inverse transforms of these functions correctly.

First, we make the definition $k_n = \mathrm{i}\mu_n$ where $\mu_n = (l^2-\gamma_n^2)^{1/2}$ when $|l|>\gamma_n$. Then it is clear that for $d_{ji}\neq 0$, all series occurring in (3.14) and (3.16) are exponentially convergent as $|l|\to\infty$. Therefore, we concentrate on the case when $j=i$ and $d_{ji}=0$. In this case, we may write

$$\left.\begin{aligned}\bar{K}_s(0,l) &= \beta\sum_{n=-2}^{\infty}\frac{g_n^2}{2\mu_n}\tau(\gamma_n)\\ \bar{L}_a(0,l) &= -\beta\sum_{n=-2}^{\infty}\frac{h_n^2}{2\mu_n}\tau(\gamma_n)\end{aligned}\right\} \tag{3.17}$$

where it was shown in the Appendix of Evans & Porter (2003) that

$$\tau(\gamma_n) = \frac{(Y_n'(0))^2}{C_n} = O(n^{-8}), \qquad \text{as } n\to\infty$$

which ensures that the series in (3.17) are convergent. We also note that $g_n = (l^2(1-\nu)-\gamma_n^2)$ and $h_n = \mu_n(l^2(1-\nu)+\gamma_n^2)$. Also, the following identities were proved in the Appendix of Evans &

Porter (2003),

$$\sum_{n=-2}^{\infty} \tau(\gamma_n) = 0, \quad \sum_{n=-2}^{\infty} \gamma_n^2 \tau(\gamma_n) = \beta^{-1} \qquad \text{and} \qquad \sum_{n=-2}^{\infty} \gamma_n^4 \tau(\gamma_n) = 0. \tag{3.18}$$

In addition to (3.17), it can be shown from (3.14) and (3.16), after some algebra, that

$$\bar{K}_a(0,l) = -\bar{L}_s(0,l) = \beta \sum_{n=-2}^{\infty} \frac{(\gamma_n^4 - (1-\nu)^2 l^4)}{2} \tau(\gamma_n) = 0$$

using (3.18). Returning to (3.17), it can be shown that

$$\frac{g_n^2}{\mu_n} = (1-\nu)^2 l^2 |l| \left(1 - \left(\frac{3+\nu}{1-\nu}\right) \frac{\gamma_n^2}{2l^2} + C(\nu) \frac{\gamma_n^4}{l^4} + O\left(\frac{1}{l^6}\right)\right), \qquad \text{as } |l| \to \infty, \text{ fixed } n \tag{3.19}$$

for some function $C(\nu)$ that we do not need to calculate. Using this in (3.17) with the identities (3.18) shows that

$$\bar{K}_s(0,l) \sim -\tfrac{1}{4}(3+\nu)(1-\nu)|l| + O(1/|l|^3), \qquad \text{as } |l| \to \infty.$$

Some care is required in taking this limit. Briefly, the summation in (3.17) must be divided into two parts, defined by the size of $|l|$, estimating the second half to be $O(1/|l|^5)$ before taking the limit $|l| \to \infty$.

A similar procedure for $\bar{L}_a(0,l)$ gives

$$\bar{L}_a(0,l) \sim -\tfrac{1}{4}(3+\nu)(1-\nu)l^2|l| + O(1/|l|), \qquad \text{as } |l| \to \infty.$$

Thus we define

$$\bar{K}_s(0,l) = -\sigma|l| + \bar{K}_s'(0,l), \qquad \bar{L}_a(0,l) = -\sigma l^2|l| + \bar{L}_a'(0,l), \tag{3.20}$$

where $\sigma = \frac{1}{4}(3+\nu)(1-\nu)$ and where $\bar{K}_s'(0,l) \sim O(1/|l|^3)$ and $\bar{L}_a'(0,l) \sim O(1/|l|)$ as $|l| \to \infty$. The form of (3.20) is in exactly the same form as in AB95 where a similar procedure was used. Although this is perhaps to be expected, the asymptotic result in AB95 was explicit from their formulation. In contrast, however, the derivation of the asymptotic results here for the more complicated case of an elastic plate bounded by a fluid has required some detailed analysis.

It follows that the inverse transforms may be written as

$$K_s(0,y) = -\frac{\sigma}{\pi}\frac{d^2}{dy^2} \ln|y| + K_s'(0,y), \qquad L_a(0,y) = \frac{\sigma}{\pi}\frac{d^4}{dy^4} \ln|y| + L_a'(0,y)$$

where

$$K_{s,a}(x,y) = \frac{1}{2\pi} \int_{-\infty}^{\infty} \bar{K}_{s,a}(x,l) \mathrm{e}^{\mathrm{i}ly} dl$$

with corresponding definitions for $L_{s,a}(x,y)$, $K_s'(x,y)$ and $L_a'(x,y)$. It is also readily shown that $K_s'(0,y) \sim |y|^3$ and $L_a'(0,y) \sim |y|$ as $y \to 0$. We note that the functions $K_{s,a}(x,y)$ are not known explicitly and will effectively be inverted numerically as part of the numerical scheme (see later equations (4.8)–(4.10)).

Returning to (3.13) and (3.15), we can implement the convolution theorem to give

$$\begin{aligned} f(c_j,y) \;=\; & -\frac{\sigma}{\pi}\frac{d^2}{dy^2} \int_{a_j^-}^{a_j^+} P_j(t) \ln|y-t| dt + \int_{a_j^-}^{a_j^+} P_j(t) K_s'(0,y-t) dt \\ & + \sum_{\substack{i=1 \\ \neq j}}^{N} \int_{a_i^-}^{a_i^+} \left\{ P_i(t) K_s(d_{ji}, y-t) + Q_i(t) K_a(d_{ji}, y-t) \right\} dt, \qquad y \in (a_j^-, a_j^+) \end{aligned} \tag{3.21}$$

and

$$g(c_j,y) = \frac{\sigma}{\pi}\frac{d^4}{dy^4}\int_{a_j^-}^{a_j^+} Q_j(t)\ln|y-t|dt + \int_{a_j^-}^{a_j^+} Q_j(t)L_a'(0,y-t)dt$$
$$+\sum_{\substack{i=1\\ \neq j}}^{N}\int_{a_i^-}^{a_i^+}\{P_i(t)L_s(d_{ji},y-t)+Q_i(t)L_a(d_{ji},y-t)\}\,dt, \qquad y\in(a_j^-,a_j^+) \tag{3.22}$$

both for $j=1,2,\ldots,N$, where

$$f(c_j,y) = -(\mathcal{B}\eta_0)(c_j,y), \qquad \text{and} \qquad g(c_j,y) = -(\mathcal{S}\eta_0)(c_j,y).$$

Also,

$$P_i(y)\equiv[\eta_x]_i = \frac{1}{2\pi}\int_{-\infty}^{\infty}\bar{P}_i(l)\mathrm{e}^{\mathrm{i}ly}dl \qquad \text{and} \qquad Q_i(y)\equiv[\eta]_i = \frac{1}{2\pi}\int_{-\infty}^{\infty}\bar{Q}_i(l)\mathrm{e}^{\mathrm{i}ly}dl$$

for $i=1,2,\ldots,N$ represent the jumps in the gradient and elevation across each of the $N$ cracks which are clearly zero if $y\notin(a_i^-,a_i^+)$.

We remark here that, when $i\neq j$ but $d_{ji}=0$ as would occur in the case of distinct parallel cracks, there is no singular behaviour in the corresponding kernels of the integral operators and no special attention is required.

The $2N$ coupled integral equations in (3.21) and (3.22) for the $2N$ unknowns $P_i(t)$, $Q_i(t)$, $i=1,2,\ldots,N$ are in a suitable form for computation. We remark that when there is only one crack, the pair of integral equations decouple into one for $P_1(t)$ and one for $Q_1(t)$.

Finally, we note from the definition of $\eta_0$ in (2.13) that

$$f(c_j,y) = (m_0^2+\nu l_0^2)\mathrm{e}^{\mathrm{i}m_0c_j}Y_0'(0)\mathrm{e}^{\mathrm{i}l_0y} \tag{3.23}$$

and

$$g(c_j,y) = \mathrm{i}m_0(m_0^2+\nu_1 l_0^2)\mathrm{e}^{\mathrm{i}m_0c_j}Y_0'(0)\mathrm{e}^{\mathrm{i}l_0y} \tag{3.24}$$

where $m_0$ and $l_0$ are defined by (2.14).

# 4 Approximation to solution of the integral equations

Guided by the analysis describing the local behaviour at the ends of cracks resulting in (2.12) we assume the following representations for the unknowns in (3.21) and (3.22)

$$P_i(t) = \frac{1}{s_i^3}\sum_{n=0}^{\infty}a_n^{(i)}\frac{\mathrm{e}^{\mathrm{i}n\pi/2}}{(n+1)}p_n^{(i)}(t), \qquad t\in(a_i^-,a_i^+) \tag{4.1}$$

and

$$Q_i(t) = \frac{2}{s_i^4}\sum_{n=0}^{\infty}b_n^{(i)}\frac{\mathrm{e}^{\mathrm{i}n\pi/2}}{(n+1)(n+2)(n+3)}q_n^{(i)}(t), \qquad t\in(a_i^-,a_i^+) \tag{4.2}$$

where

$$\left.\begin{aligned} p_n^{(i)}(t) &= \{(a_i^+-t)(t-a_i^-)\}^{1/2}U_n((t-t_i)/s_i)\\ q_n^{(i)}(t) &= \{(a_i^+-t)(t-a_i^-)\}^{3/2}C_n^{(2)}((t-t_i)/s_i)\end{aligned}\right\}$$

and where $s_i=\frac{1}{2}(a_i^+-a_i^-)$ and $t_i=\frac{1}{2}(a_i^++a_i^-)$ define the half-length and midpoint, respectively, of the $i$th crack. See figure 1. The coefficients $a_n^{(i)}$, $b_n^{(i)}$, for $i=1,2,\ldots,N$ are to be determined

and $p_n^{(i)}(t)$, $q_n^{(i)}(t)$ are weighted test functions defined in terms of $U_n(x) \equiv C_n^{(1)}(x)$ and $C_n^{(2)}(x)$ being the Chebychev polynomial of the second kind and the ultraspherical Gegenbauer polynomial, respectively. These are orthogonal polynomials which satisfy the orthogonality relationships

$$\int_{a_i^+}^{a_i^-} p_n^{(i)}(t) U_m((t-t_i)/s_i)dt = \tfrac{1}{2}\pi s_i^2 \delta_{mn};$$

$$\int_{a_i^-}^{a_i^+} q_n^{(i)}(t) C_m^{(2)}((t-t_i)/s_i)dt = \tfrac{1}{8}\pi s_i^4 (m+3)(m+1)\delta_{mn}.$$

The extra normalising factors are included in (4.1) and (4.2) for later algebraic convenience and also to ensure that $P_i(t)$ and $Q_i(t)$ are dimensionally correct.

Similar expansions were used by AB95, who also noted that the functions $U_n(x)$ and $C_n^{(2)}(x)$ may be regarded as the eigenfunctions of the singular parts of the integral equations in the sense that they satisfy

$$\frac{d^2}{dy^2}\int_{a_i^-}^{a_i^+} \ln|y-t| p_n^{(i)}(t)dt = \pi(n+1)U_n((y-t_i)/s_i) \tag{4.3}$$

and

$$\frac{d^4}{dy^4}\int_{a_i^-}^{a_i^+} \ln|y-t| q_n^{(i)}(t)dt = -\pi(n+3)(n+2)(n+1)C_n^{(2)}((y-t_i)/s_i) \tag{4.4}$$

for $y \in (a_i^-, a_i^+)$ (note that AB95 have omitted a minus sign in error in their version of (4.4)).

In what follows, we will also make use of the results

$$\int_{a_i^-}^{a_i^+} \mathrm{e}^{ilt} p_n^{(i)}(t)dt = \frac{\mathrm{e}^{\mathrm{i}lt_i}\mathrm{e}^{\mathrm{i}n\pi/2}(n+1)\pi s_i^2}{ls_i} J_{n+1}(ls_i) \tag{4.5}$$

and

$$\int_{a_i^-}^{a_i^+} \mathrm{e}^{ilt} q_n^{(i)}(t)dt = \frac{\mathrm{e}^{\mathrm{i}lt_i}\mathrm{e}^{\mathrm{i}n\pi/2}(n+3)(n+2)(n+1)\pi s_i^4}{2(ls_i)^2} J_{n+2}(ls_i). \tag{4.6}$$

(see for example, Gradshteyn & Ryzhik (1981)) where $J_n(z)$ is the Bessel function.

A Galerkin method is used to transform the coupled integral equations (3.21) and (3.22) into a coupled linear system of algebraic equations for the coefficients $a_n^{(i)}$, $b_n^{(i)}$. To summarise this process, we substitute (4.1) and (4.2) into (3.21) and (3.22), multiply through the first of these by $p_m^{(j)}(y)$ and the second by $q_m^{(j)}(y)$ and integrate over $a_j^- < y < a_j^+$.

Thus, after substituting (4.1) and (4.2) into (3.21) we find that

$$\begin{aligned} f(c_j, y) \;=\; & -\frac{\sigma}{s_j^3}\sum_{n=0}^{\infty} a_n^{(j)} \mathrm{e}^{\mathrm{i}n\pi/2} U_n((y-t_j)/s_j) + \frac{1}{2s_j}\sum_{n=0}^{\infty} a_n^{(j)} \int_{-\infty}^{\infty} \bar{K}_s'(0,l)\mathrm{e}^{\mathrm{i}l(y-t_j)} \frac{J_{n+1}(ls_j)}{ls_j} dl \\ & + \sum_{\substack{i=1 \\ \neq j}}^{N} \frac{1}{2s_i}\sum_{n=0}^{\infty} a_n^{(i)} \int_{-\infty}^{\infty} \bar{K}_s(d_{ji}, l)\mathrm{e}^{\mathrm{i}l(y-t_i)} \frac{J_{n+1}(ls_i)}{ls_i} dl \\ & + \sum_{\substack{i=1 \\ \neq j}}^{N} \frac{1}{2}\sum_{n=0}^{\infty} b_n^{(i)} \int_{-\infty}^{\infty} \bar{K}_a(d_{ji}, l)\mathrm{e}^{\mathrm{i}l(y-t_i)} \frac{J_{n+2}(ls_i)}{(ls_i)^2} dl \end{aligned}$$

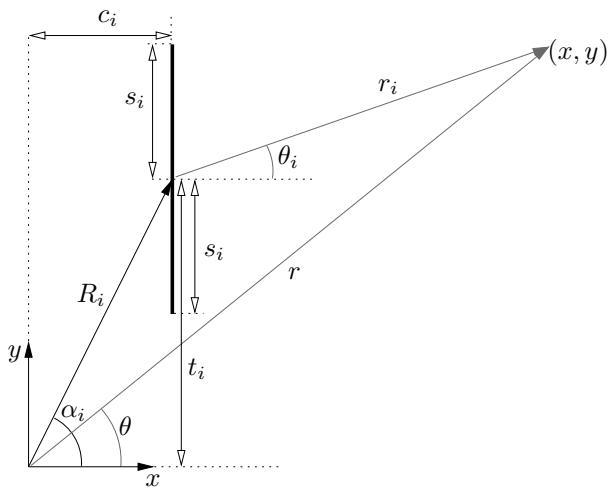


Figure 1: Definition of geometrical parameters used to define the $i$th crack

where (4.3)–(4.6) have been used. After multiplying through by $p_m^{(j)}(y)$ and integrating over $a_j^- < y < a_j^+$ we find, after considerable algebra, that

$$F_m^{(j)} = \frac{-\sigma}{(m+1)} a_m^{(j)} + \sum_{n=0}^{\infty} a_n^{(j)} K_{s,(mn)}^{\prime(j)} + \sum_{\substack{i=1 \\ \neq j}}^{N} \sum_{n=0}^{\infty} \left( a_n^{(i)} K_{s,(mn)}^{(ij)} + b_n^{(i)} K_{a,(mn)}^{(ij)} \right) \tag{4.7}$$

for $j = 1, 2, \ldots, N$, $m = 0, 1, \ldots$. Here,

$$K_{s,(mn)}^{\prime(j)} = \int_{-\infty}^{\infty} \{ s_j \bar{K}_s'(0, l) \} \frac{J_{n+1}(ls_j) J_{m+1}(ls_j)}{(ls_j)^2} d(ls_j) \tag{4.8}$$

$$K_{s,(mn)}^{(ij)} = \int_{-\infty}^{\infty} \{ s_j \bar{K}_s(d_{ji}, l) \} \mathrm{e}^{\mathrm{i}l(t_j - t_i)} \frac{J_{n+1}(ls_i) J_{m+1}(ls_j)}{(ls_i)^2} d(ls_j) \tag{4.9}$$

and

$$K_{a,(mn)}^{(ij)} = \int_{-\infty}^{\infty} \{ s_j^2 \bar{K}_a(d_{ji}, l) \} \mathrm{e}^{\mathrm{i}l(t_j - t_i)} \frac{J_{n+2}(ls_i) J_{m+1}(ls_j)}{(ls_i)^2 (ls_j)} d(ls_j) \tag{4.10}$$

where the terms in braces are non-dimensional. Also,

$$\begin{aligned} F_m^{(j)} &= \frac{2 s_j \mathrm{e}^{-\mathrm{i}m\pi/2}}{\pi(m+1)} \int_{a_j^-}^{a_j^+} f(c_j, y) p_m^{(j)}(y) dy \\ &= 2 s_j^3 (m_0^2 + \nu l_0^2) Y_0'(0) \mathrm{e}^{\mathrm{i}(m_0 c_j + l_0 t_j)} \frac{J_{m+1}(l_0 s_j)}{(l_0 s_j)} \end{aligned} \tag{4.11}$$

using the definition of $f(c_j, y)$ in (3.23) and (4.5).

We follow the same steps for the treatment of (3.21). Thus, substitution of (4.1) and (4.2) gives, after some tidying up

$$\begin{aligned} g(c_j, y) = &- \frac{2\sigma}{s_j^4} \sum_{n=0}^{\infty} b_n^{(j)} \mathrm{e}^{\mathrm{i}n\pi/2} C_n^{(2)}((y - t_j)/s_j) + \frac{1}{4} \sum_{n=0}^{\infty} b_n^{(j)} \int_{-\infty}^{\infty} \bar{L}_a'(0, l) \mathrm{e}^{\mathrm{i}l(y - t_j)} \frac{J_{n+2}(ls_j)}{(ls_j)^2} dl \\ &+ \sum_{\substack{i=1 \\ \neq j}}^{N} \frac{1}{2s_i} \sum_{n=0}^{\infty} a_n^{(i)} \int_{-\infty}^{\infty} \bar{L}_s(d_{ji}, l) \mathrm{e}^{\mathrm{i}l(y - t_i)} \frac{J_{n+1}(ls_i)}{ls_i} dl \end{aligned}$$

$$+\sum_{\substack{i=1\\ \neq j}}^{N}\frac{1}{2}\sum_{n=0}^{\infty}b_n^{(i)}\int_{-\infty}^{\infty}\bar{L}_a(d_{ji},l)\mathrm{e}^{\mathrm{i}l(y-t_i)}\frac{J_{n+2}(ls_i)}{(ls_i)^2}dl$$

Multiplication by $q_m^{(j)}(y)$ and integration over $a_j^- < y < a_j^+$ results in

$$G_m^{(j)} = -\frac{\sigma}{(m+2)}b_m^{(j)} + \sum_{n=0}^{\infty}b_n^{(j)}L_{a,(mn)}^{\prime(j)} + \sum_{\substack{i=1\\ \neq j}}^{N}\sum_{n=0}^{\infty}\left(a_n^{(i)}L_{s,(mn)}^{(ij)} + b_n^{(i)}L_{a,(mn)}^{(ij)}\right) \tag{4.12}$$

for $j = 1, 2, \ldots, N$, $m = 0, 1, \ldots$ where

$$L_{a,(mn)}^{\prime(j)} = \int_{-\infty}^{\infty}\{s_j^3\bar{L}_s'(0,l)\}\frac{J_{n+2}(ls_j)J_{m+2}(ls_j)}{(ls_j)^4}d(ls_j) \tag{4.13}$$

$$L_{s,(mn)}^{(ij)} = \int_{-\infty}^{\infty}\{s_j^2\bar{L}_s(d_{ji},l)\}\mathrm{e}^{\mathrm{i}l(t_j-t_i)}\frac{J_{n+1}(ls_i)J_{m+2}(ls_j)}{(ls_i)^2(ls_j)}d(ls_j) \tag{4.14}$$

and

$$L_{a,(mn)}^{(ij)} = \int_{-\infty}^{\infty}\{s_j^3\bar{L}_a(d_{ji},l)\}\mathrm{e}^{\mathrm{i}l(t_j-t_i)}\frac{J_{n+2}(ls_i)J_{m+2}(ls_j)}{(ls_i)^2(ls_j)^2}d(ls_j) \tag{4.15}$$

As before, the braces include non-dimensional quantities. Finally,

$$\begin{aligned} G_m^{(j)} &= \frac{4s_j\mathrm{e}^{-\mathrm{i}m\pi/2}}{\pi(m+1)(m+2)(m+3)}\int_{a_j^-}^{a_j^+}g(c_j,y)q_m^{(j)}(y)dy \\ &= 2\mathrm{i}s_j^4m_0(m_0^2+\nu_1l_0^2)Y_0'(0)\mathrm{e}^{\mathrm{i}(m_0c_j+l_0t_j)}\frac{J_{m+2}(l_0s_j)}{(l_0s_j)^2} \end{aligned} \tag{4.16}$$

using the definition of $g(c_j, y)$ in (3.24) and (4.6).

In terms of numerical implementation, advantage can be taken of various symmetry relations including $s_i^4K_{s,(mn)}^{(ij)} = -(-1)^{m+n}s_j^4K_{s,(nm)}^{(ji)}$, and $s_i^4L_{s,(mn)}^{(ij)} = (-1)^{m+n}s_j^4K_{a,(nm)}^{(ji)}$ for example, which follow from relations (3.14), (3.16).

Notice also that the positioning of each crack, with centres $(c_i, t_i)$ occur as differences in exponentials in the combinations $\mathrm{e}^{\mathrm{i}k_n|c_j-c_i|}\mathrm{e}^{\mathrm{i}l(t_j-t_i)}$. This means that the $i \neq j$ terms essentially contain information about the relative distance and orientation of each of the cracks with respect to one another rather than each to some fixed origin of reference, whilst the sizes of the cracks appear separately as other multiplying terms. This, of course, is not surprising and it allows one to identify the wave interaction effects between each pair of cracks from these terms. In particular, one might be inclined to make a simplifying approximation, akin to the well-known wide-spacing approximation, in which only the propagating wave modes are retained in the interaction between two 'widely' separated cracks. In this case it is clear that one disgards all but the $n = 0$ mode in the infinite sums which define the transform functions $\bar{K}_{s,a}(d_{ji}, l)$, $\bar{L}_{s,a}(d_{ji}, l)$. However, there is little to be gained by such a procedure as there is no further analytic progress that could be made and the numerical savings are not especially significant.

# 5 Far-field diffracted wave amplitudes

The first task here is to represent the transforms of the functions $P_i(y)$ and $Q_i(y)$ in terms of the coefficients $a_n^{(i)}$ and $b_n^{(i)}$ introduced in (4.1) and (4.2). Thus, we find using (4.5) that

$$\bar{P}_i(l) = \int_{a_i^-}^{a_i^+}P_i(y)\mathrm{e}^{-\mathrm{i}ly}dy = \mathrm{e}^{-\mathrm{i}lt_i}\frac{\pi}{s_i}\sum_{n=0}^{\infty}a_n^{(i)}\frac{J_{n+1}(ls_i)}{ls_i} \tag{5.1}$$

and using (4.6) that

$$\bar{Q}_i(l) = \int_{a_i^-}^{a_i^+} Q_i(y)\mathrm{e}^{-\mathrm{i}ly}dy = \mathrm{e}^{-\mathrm{i}lt_i}\pi\sum_{n=0}^{\infty} b_n^{(i)}\frac{J_{n+2}(ls_i)}{(ls_i)^2}. \tag{5.2}$$

Far away from the cracks, the wave field is a superposition of the incident plane wave, $\phi_0$, and components of the diffracted field from each of the cracks. Thus we write the latter part as

$$\phi_d(r,\theta,z) = \phi - \phi_0 \sim \sum_{i=1}^{N}\Big(U_i(r,\theta) + V_i(r,\theta)\Big)Y_0(z), \qquad \text{as } r\to\infty \tag{5.3}$$

where $r = (x^2+y^2)^{\frac{1}{2}}$ and $x = r\cos\theta$, $y = r\sin\theta$. Here, we have anticipated the fact that only the terms proportional to $Y_0(z)$ will contribute to the wave field at large distances and written

$$U_i(r,\theta) \equiv U_i(r_i,\theta_i) = \lim_{r_i\to\infty}\frac{\mathrm{i}\beta Y_0'(0)}{4\pi C_0}\int_{-\infty}^{\infty}\frac{g_0}{k_0}\mathrm{e}^{\mathrm{i}lt_i}\bar{P}_i(l)\mathrm{e}^{\mathrm{i}k_0r_i|\cos\theta_i|}\mathrm{e}^{\mathrm{i}lr_i\sin\theta_i}dl \tag{5.4}$$

and

$$V_i(r,\theta) \equiv V_i(r_i,\theta_i) = \lim_{r_i\to\infty}\frac{-\mathrm{i}\beta Y_0'(0)}{4\pi C_0}\int_{-\infty}^{\infty}\frac{h_0}{k_0}\mathrm{e}^{\mathrm{i}lt_i}\bar{Q}_i(l)\mathrm{sgn}(x-c_i)\mathrm{e}^{\mathrm{i}k_0r_i|\cos\theta_i|}\mathrm{e}^{\mathrm{i}lr_i\sin\theta_i}dl \tag{5.5}$$

and defined $x-c_i = r_i\cos\theta_i$, $y-t_i = r_i\sin\theta_i$. These represent polar coordinates based on the centre of the $i$th crack (see figure 2). There is clearly a relationship between the global polar coordinate system $(r,\theta)$ and each of the local coordinate systems $(r_i,\theta_i)$, $i = 1,2,\ldots,N$ but we do not need to know these explicitly. Instead, we note that as $r\to\infty$

$$\theta_i \to \theta, \qquad \text{and} \qquad r_i \to r - R_i\cos(\alpha_i-\theta) \tag{5.6}$$

where $R_i = (c_i^2+t_i^2)^{\frac{1}{2}}$, $\alpha_i = \tan^{-1}(t_i/c_i)$. As a passing remark, note that the argument of the exponentials in (4.11) and (4.16), namely $\mathrm{i}(m_0c_j + l_0t_j)$ can now be written as $\mathrm{i}\gamma_0R_j\cos(\alpha_j-\theta_{inc})$ where (2.14) has been used and $\theta_{inc}$ is the incident wave angle.

Returning to (5.4) and (5.5), we note the symmetry relations $U_i(r_i,\theta_i) = U_i(r_i,\pi-\theta_i)$ and $V_i(r_i,\theta_i) = -V_i(r_i,\pi-\theta_i)$, which means that each expression needs only be considered for $-\frac{1}{2}\pi < \theta_i < \frac{1}{2}\pi$.

We make the change of variable $l = \gamma_0\sin w$, implying that $k_0 = \gamma_0\cos w$, where $w$ is a complex number. Then, for example in (5.4), we have

$$U_i(r_i,\theta_i) = \lim_{r_i\to\infty}\frac{-\mathrm{i}\beta Y_0'(0)}{4\pi C_0}\int_{\mathcal{C}}\gamma_0^2(\cos^2 w + \nu\sin^2 w)\mathrm{e}^{\mathrm{i}\gamma_0t_i\sin w}\bar{P}_i(\gamma_0\sin w)\mathrm{e}^{\mathrm{i}\gamma_0r_i\cos(\theta_i-w)}dw$$

and the contour $\mathcal{C}$ is comprised of the three straight line segments $\mathcal{C}_1\cup\mathcal{C}_2\cup\mathcal{C}_3$ where $\mathcal{C}_1 := \{-\frac{1}{2}\pi+\theta_i < w < -\frac{1}{2}\pi+\theta_i+\mathrm{i}\infty\}$, $\mathcal{C}_2 := \{-\frac{1}{2}\pi+\theta_i < w < \frac{1}{2}\pi+\theta_i\}$, and $\mathcal{C}_3 := \{\frac{1}{2}\pi+\theta_i-\mathrm{i}\infty < w < \frac{1}{2}\pi+\theta_i\}$. As $r_i\to\infty$, the dominant contribution to the integral is from the saddle point at $w=\theta_i$ which is calculated by steepest descent to give

$$U_i(r_i,\theta_i) = \left(\frac{2\pi}{\gamma_0r_i}\right)^{1/2}\mathrm{e}^{\mathrm{i}\gamma_0r_i-\mathrm{i}\pi/4}\left\{\frac{-\mathrm{i}\beta Y_0'(0)}{4\pi C_0}\gamma_0^2(\cos^2\theta_i+\nu\sin^2\theta_i)\mathrm{e}^{i\gamma_0t_i\sin\theta_i}\bar{P}_i(\gamma_0\sin\theta_i)\right\}.$$

A similar analysis for $V_i(r_i,\theta_i)$ shows that

$$V_i(r_i,\theta_i) = \left(\frac{2\pi}{\gamma_0r_i}\right)^{1/2}\mathrm{e}^{\mathrm{i}\gamma_0r_i-\mathrm{i}\pi/4}\left\{-\frac{\beta Y_0'(0)}{4\pi C_0}\gamma_0^3\cos\theta_i(\cos^2\theta_i+\nu_1\sin^2\theta_i)\mathrm{e}^{i\gamma_0t_i\sin\theta_i}\bar{Q}_i(\gamma_0\sin\theta_i)\right\}.$$

Bringing these results together in (5.3) using (5.6) gives

$$\phi_d(r,\theta,z) \sim \left(\frac{2\pi}{\gamma_0 r}\right)^{1/2} \mathrm{e}^{\mathrm{i}\gamma_0 r - \mathrm{i}\pi/4} Y_0(z) A(\theta), \qquad \text{as } r \to \infty \tag{5.7}$$

where the diffraction coefficient is defined as

$$A(\theta) = \frac{\beta\gamma_0^2 Y_0'(0)}{4\pi C_0} \sum_{i=1}^{N} \Big\{ -\mathrm{i}(\cos^2\theta + \nu\sin^2\theta)\mathrm{e}^{\mathrm{i}\gamma_0 t_i \sin\theta} \bar{P}_i(\gamma_0 \sin\theta) \\ -\gamma_0 \cos\theta(\cos^2\theta + \nu_1 \sin^2\theta)\mathrm{e}^{\mathrm{i}\gamma_0 t_i \sin\theta} \bar{Q}_i(\gamma_0 \sin\theta) \Big\} \mathrm{e}^{-\mathrm{i}\gamma_0 R_i \cos(\alpha_i - \theta)}. \tag{5.8}$$

This expression can be posed in terms of the coefficients $a_n^{(i)}$ and $b_n^{(i)}$ after substituting from (5.1) and (5.2) whence it can be noticed that the resulting expressions can be written in terms of $R_i$ and $\alpha_i$ and not explicitly on $t_i$.

### 5.1 An energy relation

An expression for representing conservation of energy can be found by using Green's identity with the function $\phi$ and $\phi^*$. A lengthy calculation leads to

$$\Sigma = \frac{1}{2\pi}\int_0^{2\pi} |A(\theta)|^2 d\theta = -\frac{1}{\pi}\Re\{A(\theta_{inc})\} \tag{5.9}$$

where $\Sigma$ is often referred to as the scattering cross-section. The result (5.9) is well-known and applies in many wave scattering theories (e.g. in optics, acoustics, electromagnetics) where it is referred to as an 'optical theorem'. In the context of thin elastic plates under fluid loading the optical theorem has been derived by, for example, Belinsky & Kouzov (1980), Belinsky (1982) and more recently by Norris & Vermula (1995).

## 6 Stress intensity at the edges of the cracks

An important quantity in determining the possibility of dynamic fracture at one end of a crack is the stress intensity factor (see, for example, Hertzberg (1996)). According to the mathematical model, the stress at the tip of the crack is unbounded, although the model does not allow for the plastic deformation which occurs at the edge of the crack. Thus, the stress intensity factor is defined by

$$K_i^{\pm} = \lim_{y \to a_i^{\pm}} \sqrt{\pm 2\pi(y - a_i^{\pm})}\sigma_x(c_i, y)$$

where $\sigma_x(c_i, y)$ is the lateral stress along $x = c_i$ and the limits are approached from below $a_i^-$ and above $a_i^+$ (i.e. from within the elastic plate). If the value of $K_i^{\pm}$ exceeds a particular critical value, usually determined experimentally, then it is likely that there will be a fracture occur at the tip of the crack. Here, the stress is given by (Timoshenko & Woinowsky-Krieger (1959))

$$\sigma_x = \frac{Ed}{2(1-\nu^2)}\left(\nu\frac{\partial^2\eta}{\partial x^2} + \frac{\partial^2\eta}{\partial y^2}\right).$$

On account of the definition of $K_i^{\pm}$, it is only the most singular part of the stress which contributes. In a similar manner to the development of the integral equations seen earlier, we find after lengthy algebra that

$$\sigma_x(c_i, y) \sim \frac{3Ed(1-\nu)}{8(1+\nu)}\left(-\frac{1}{\pi}\frac{\mathrm{d}^2}{\mathrm{d}y^2}\int_{a_i^-}^{a_i^+} \ln|y-t| P_i(t)\mathrm{d}t\right)$$

plus bounded terms. Using the expansion for $P_i(t)$, changes of variables in $y$ and $t$, and the result (see, for example, AB95) valid for $|y| > 1$

$$-\frac{1}{\pi}\frac{\mathrm{d}^2}{\mathrm{d}y^2}\int_{-1}^{1}\ln|y-t|(1-t^2)^{1/2}U_n(t)\mathrm{d}t = \frac{|y|}{(1-y^2)^{1/2}}U_n(y) \\ +\mathrm{sgn}(y)(1-y^2)^{1/2}U_n'(y) - \tfrac{1}{2}(n+1)U_n(y)$$

it can be shown that

$$K_i^{\pm} = \mathrm{i}\sqrt{\frac{\pi}{s_i}}\left(\frac{3Ed(1-\nu)}{8s_i^2(1+\nu)}\right)\sum_{n=0}^{\infty}a_n^{(i)}\mathrm{e}^{\pm in\pi/2}. \tag{6.1}$$

# 7 Numerical results

Results are obtained by computing coefficients $a_n^{(i)}$, $b_n^{(i)}$ from the truncated version of the coupled infinite system of equations in (4.7) and (4.12). The truncation size reflects the number of terms used in the expansion of the functions representing the jumps in gradient and elevation across the crack. These functions have been chosen to incorporate the correct behaviour at the ends of the crack, and therefore only a small number of terms are needed for a high degree of accuracy in quantities of interest. The number of terms required depends upon the incident wavenumber $\gamma_0$ and the length of the crack $2s_i$, $i = 1, \ldots, N$; larger values of $\gamma_0 s_i$ require more terms than smaller values. Typically, only five terms are required, and in the most extreme cases considered here ten terms are used, with a view to achieving at least three decimal places accuracy in quantities of interest at all times. The equations (4.7) and (4.12) require the computation of infinite integrals, all of which can be transformed into semi-infinite integrals. The convergence of these integrals can also be calculated using the asymptotics of Bessel functions for large argument, along with the large $|l|$ asymptotics for the infinite sums, previously discussed in relation to determining the inversion of the Fourier transforms in section 3. Thus, integrals can be accurately and efficiently calculated by truncation to an appropriate upper limit.

The energy relation (5.9) is successfully used as a check of the accuracy of computed results, though the integral defining the left-hand side of (5.9) must inevitably be approximated. Indication from numerical experiments suggests that (5.9) is automatically satisfied by the formulation and should not be used as an indication of convergence of the results as a function of truncation size. This is a common feature of problems posed in terms of integral equations and approximated using Galerkin methods (see Porter (1995) for example).

For all results presented, the following values for physical parameters are used: $E = 5 \times 10^9$Pa, $\nu = 0.3$, $\rho_w = 1025\mathrm{kgm}^{-3}$, $\rho_p = 925.5\mathrm{kgm}^{-3}$, $g = 9.81\mathrm{ms}^{-2}$, $d = 1$m, $h = 40$m. Varying the ice thickness or the water depth leads to the same qualitative behaviour in the results (see Evans & Porter (2003) for example). The range of wavelengths to be considered varies from $\lambda = 50$m to $\lambda = 200$m, which translates into a range of (non-dimensional) incident wavenumbers from $\gamma_0 d = 0.1256$ to $\gamma_0 d = 0.0314$ respectively. These parameter values are within the range for ice sheets suggested by Squire *et al* (1995).

The first case we consider is the simplest, being wave interaction with a single crack. For illustrative purposes we take the crack to be 200m in length, the same length as the maximum wavelength and four times the shortest wavelength considered. In order to illustrate as much qualitative behaviour as possible, we present in figures 2-3 three-dimensional plots, each measuring the modulus of the diffraction coefficient, $|A(\theta)|$ as a function of observation angle $\theta$ and one other variable. In the first set of two figures 2(a,b) we show the variation in $|A(\theta)|$ with $\gamma_0 d$ for the case of (a) $\theta_{inc} = 0^\circ$ (hereafter referred to as "beam" incidence) and (b) $\theta_{inc} = 90^\circ$ (referred to as "head" incidence). In each case, only half of the $\theta$ range is required as there is symmetry with $\theta$ in $|A(\theta)|$. As expected, there is significantly more energy diffracted under beam incidence than for

head incidence, and this energy is mainly propagated in the directions around $\theta = 0$ and $\theta = \pi$. For head incidence, the diffracted wave energy has a more complex structure as a function of $\theta$, especially as the wavenumber $\gamma_0 d$ is increased.

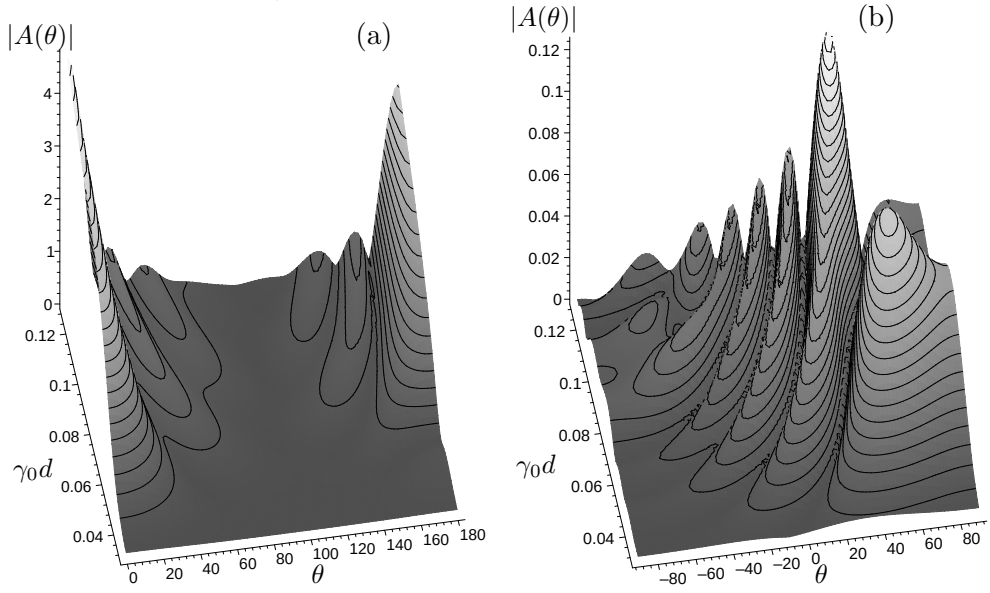


Figure 2: The diffraction coefficient, $|A(\theta)|$, as a function of $\gamma_0 d$ for a crack of length 200m with (a) $\theta_{inc} = 0°$ and (b) $\theta_{inc} = 90°$.

In figures 3(a),(b) we show the variation of $|A(\theta)|$ as a function of $\theta$ with varying $\theta_{inc}$ for values of (a) $\gamma_0 d = 0.0628$ ($\lambda = 100$m) and (b) $\gamma_0 d = 0.1256$ ($\lambda = 50$m). In each case, only the range $0° \leq \theta_{inc} \leq 90°$ (from beam incidence around to head incidence) needs to be considered due to the symmetries in the geometry. In both figures, the most wave energy is diffracted along the directions $\theta = \theta_{inc}$ and $\theta = \pi - \theta_{inc}$ which correspond to the reflected and transmitted wave angles for an infinitely long crack. At the higher frequency (figure 3), the diffracted wave energy is more focussed along these lines, as might be expected.

A snapshot in time of the plate elevation for the diffracted part of the wave, $\eta_d$ is given in figures 4, 5 in the case of a single crack. The total wave field requires the superposition of the incident wave field $\eta_{inc}$, which is assumed to have unit amplitude. In both cases, symmetry in the diffraction wave pattern means that only half the plate needs to be plotted, and this allows us to illustrate the elevation of the plate along the cracks. In figure 4, we consider high-frequency beam incidence upon a crack of length 50m. Most of the diffracted wave energy is along $\theta = 0$ and $\theta = 180°$. The maximum plate elevation occurs along each side of the crack, and in this example is over three times the amplitude of the incidence wave.

In figure 5 a crack of length 200m is under head incidence and now we can observe the plate elevation along the edge of the crack $x = 0$, $-100 < y < 100$. Here, the plate elevation is symmetrical about $x = 0$. The feature to note here, common in a range of similar examples computed numerically, is the large peaks in the plate elevation at the two ends of the cracks. The diffracted wave energy is scattered over a range of angles, with very little reflected back towards the source.

There are many different configurations of cracks that we might consider. With two cracks, the most interesting effects occur when one crack is placed directly behind the other, as this introduces the possibility of resonance in the strip between the two cracks. To illustrate this effect, in figure 6 we consider the case of beam incidence upon two cracks, both 100m in length, with $t_i = 0$ and when separated by various distances $b = c_2 - c_1$ ranging from 40m down to just 2.5m. The maximum

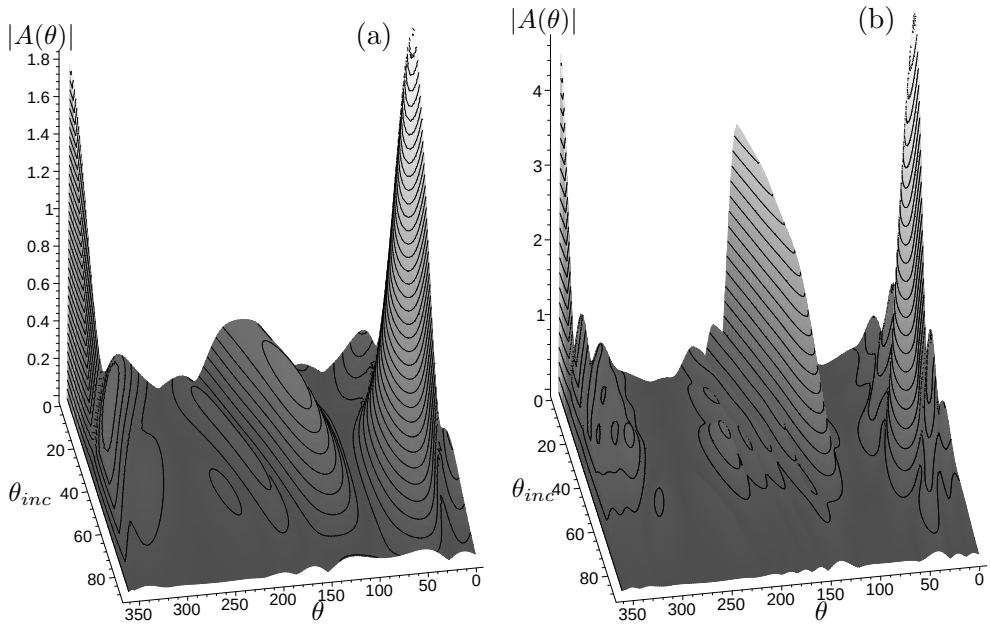


Figure 3: The diffraction coefficient, $|A(\theta)|$, as a function of $\theta_{inc}$ for a crack of length 200m with (a) $\gamma_0 d = 0.0628$ and (b) $\gamma_0 d = 0.1256$.

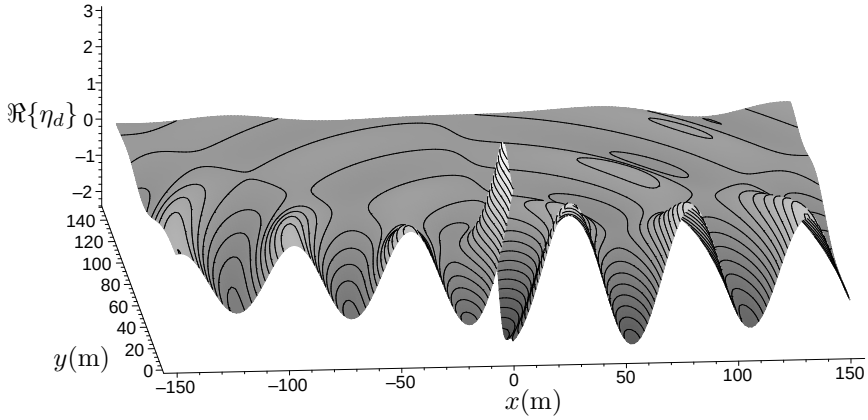


Figure 4: Snapshot of diffracted part of the plate elevation for a crack, length 100m, under beam incidence, $\gamma_0 d = 0.1256$ ($\lambda = 50$m).

plate elevation occurs along $y = 0$ and between the two cracks (illustrated, for example, in figure 7 for a separation of 20m) and this is plotted in figure 6 as $\gamma_0 d$ is varied. As the separation between the cracks is reduced, a primary peak in the resonant amplitude is formed which increases in size dramatically. A secondary peak also forms at higher values of $\gamma_0 d$, but only for closely-separated cracks. Perhaps the most interesting aspect of these plots is the size of the resonant amplitude for fairly modest separations and also the broadness of the peak over a large range of values of $\gamma_0 d$. For example, with $b = 10$m, the maximum amplitude of the plate between the cracks is over four times the incident wave amplitude for all wavelengths between 50m and 110m.

The modulus of the stress intensity factor (SIF), $|K_1^{\pm}|$ associated with the ends of the cracks for a single crack as a function of wavenumber $\gamma_0 d$ is plotted in figure 8. The SIF is dimensional and the large values taken by $|K_1^{\pm}|$ in figure 8 is due mainly to the its dependence on Young's modulus, $E$. In figure 8(a) the dependence of the SIF on crack length is shown for symmetric beam-incident

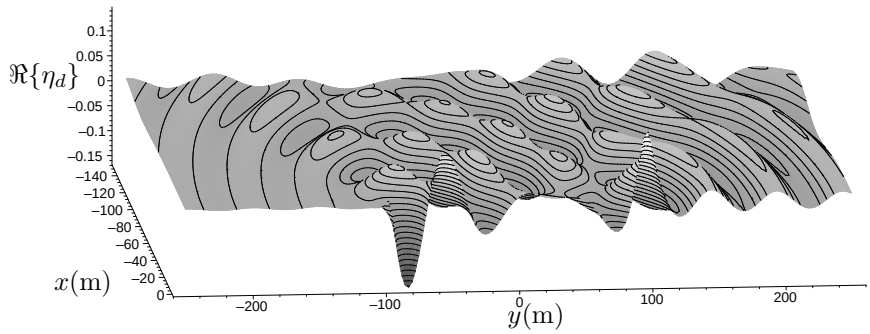


Figure 5: Snapshot of diffracted part of the plate elevation for a crack, length 200m, under head incidence, $\gamma_0 d = 0.1256$ ($\lambda = 50$m).

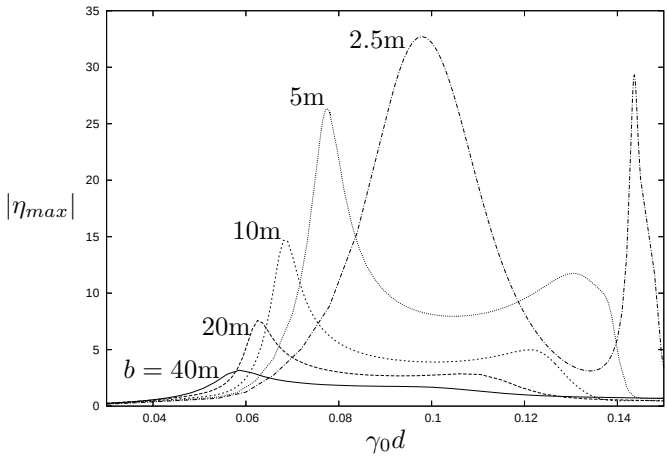


Figure 6: The maximum plate elevation $|\eta_{max}|$ as a function of wavenumber $\gamma_0 d$ for two aligned parallel cracks, each of length 100m under beam incidence and various spacings, $b = c_2 - c_1$ (shown against curves).

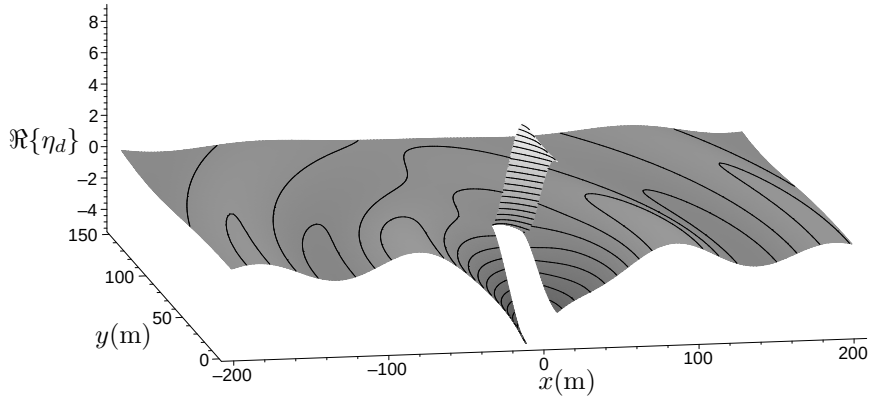


Figure 7: Snapshot of diffracted part of the plate elevation for two aligned parallel cracks, length 100m, separated by 20m under beam incidence at resonance, $\gamma_0 d = 0.0628$, ($\lambda = 100$m).

waves. As expected, the SIF associated with each crack tip rapidly becomes independent of the length of the crack as it is increased. This is more apparent at larger values of $\gamma_0 d$ (smaller wavelengths), again as expected. This result might allow us to speculate that, for the particular

set of parameters being considered in this numerical experiment, the response at the centre of a crack of length 100m would be close to that for an infinitely long crack.

In figure 8(b) the effect of the incident wave angle on the SIF at the near and far ends of a single crack of fixed length 100m is shown. At beam incidence, the SIF at the two ends of the crack are, of course, identical.

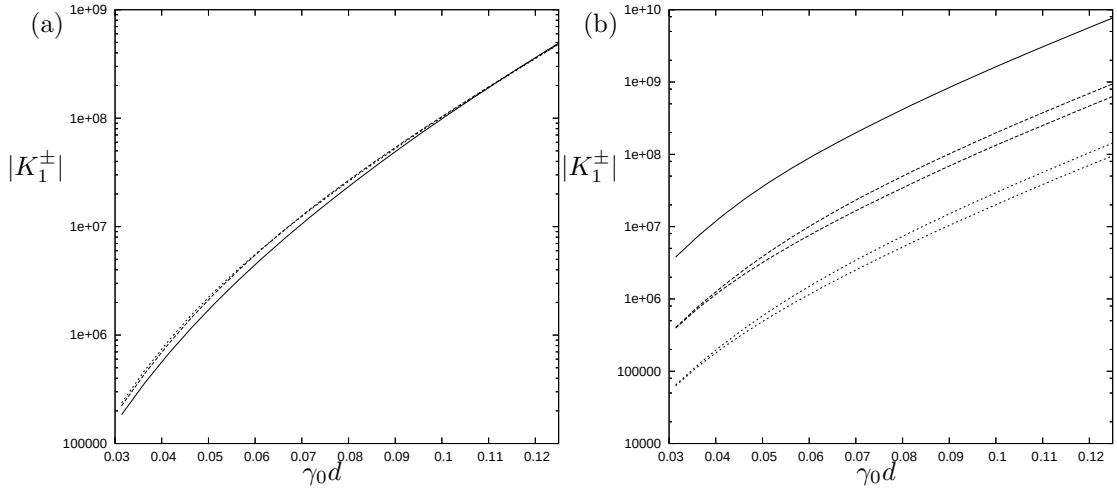


Figure 8: The stress insensity factors associated with crack tips as $\gamma_0 d$ varies for: (a) a single crack of length 25m (solid), 50m (long dash), 100m (dotted) under beam incidence; (b) a crack of length 100m for beam incidence (solid line), 45° incidence (dashed lines - upper/lower lines near/far cracks) and head incidence (dotted lines - upper/lower lines are near/far cracks).

Finally, in figure 9 we show illustrative results for four cracks, in this case randomly arranged and under oblique incidence; see figure caption for details. A plan view shows a snapshot in time of the diffracted wave relief as different shades of black of white. The incident wave angle is 45°, and it can be seen that the primary scattering angles, as expected, for this relatively high-frequency wave is at 45° and 135°. This is because a dominant part of the wave diffraction is wave reflection from, and transmission beyond, the cracks. A lesser component of the wave diffraction is due to the end effects of the cracks.

# 8 Conclusion

In this paper we have shown how the problem of wave scattering of an incident plane wave by narrow straight-line cracks in an elastic sheet floating on water can be formulated in terms of integral equations for functions related to the jumps in slope and displacement across the cracks. These integral equations are shown to have hypersingular kernels. The numerical method for computing their solution uses a Galerkin approach in conjunction with certain orthogonal functions. These functions incorporate the physical nature of the solution at the ends of the crack, as well as allowing explicit integration of the singular components of the integral equations.

The current problem is a significant extension of the large body of previous work which has considered the two-dimensional problem of wave transmission beyond *infinitely long* straight-line cracks, in that the effect of crack terminations on wave propagation are included. Simple expressions have been derived for the stress intensity factors associated with the ends of the cracks. These factors are important in determining the onset of fracture, which may occur once the factors exceed an experimentally determined critical value.

The canonical problem involving crack terminations is one in which waves are incident upon a

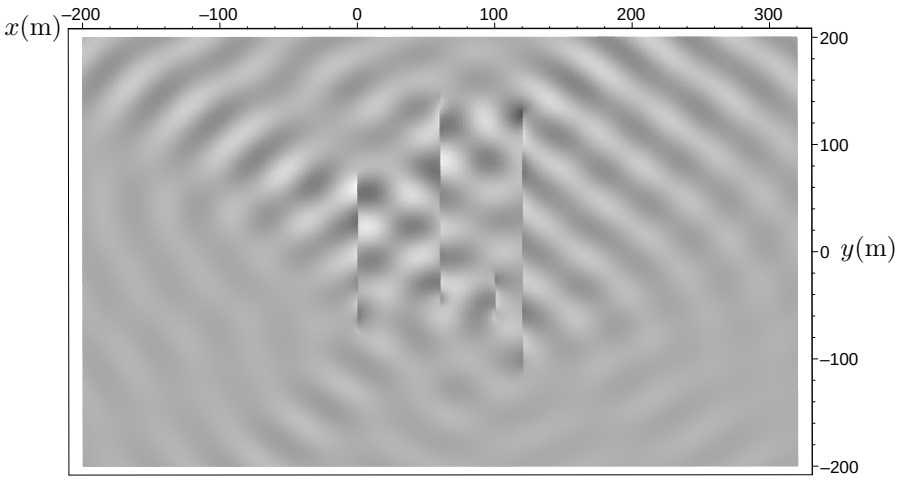


Figure 9: Plan view relief snapshot of the diffracted part of the plate elevation for four cracks ($c_1 = 0$m, $t_1 = 0$m, $s_1 = 75$m; $c_2 = 60$m, $t_2 = 50$m, $s_2 = 100$m; $c_3 = 100$m, $t_3 = -40$m, $s_2 = 25$m; $c_4 = 120$m, $t_4 = 10$m, $s_4 = 125$m) with $\gamma_0 d = 0.141$ under oblique incidence $\theta_{inc} = 45°$.

crack of semi-infinite extent. Here, an analogous problem exists in the *in vacuo* case, namely the scattering of flexural waves by a semi-infinite crack in an elastic sheet, and has been previously been considered by Norris & Wang (1994). They used a Wiener-Hopf approach in the solution of the problem and paid particular attention to the wave energy which is fed into the form of 'edge waves' which propagate to infinity along the free edges of the crack. Such edge waves are well-known and explicit for a plate *in vacuo*, and analogous edge waves for a crack in an elastic plate over water were shown to exist numerically by Evans & Porter (2003). Thus, there remains the possibility of extending the work of Norris & Wang (1994) to the case of an elastic sheet having a semi-infinite crack bounded below by fluid. Preliminary work suggests that the solution of this problem is requires a Wiener-Hopf split function not defined explicitly, but as a parameter in the integrand of a Fourier-type integral which greatly complicates the solution.

A further generalisation of the current work involves the scattering of waves by cracks of arbitrary shape and orientation. Here, analytic progress has been made by the authors and this will take the form of a subsequent publication, although some preliminary details of the method have previously been reported in Porter & Evans (2004).

### Acknowledgements

The authors would like to thank the anonymous referees for their useful, perceptive and detailed comments at the review stage of this paper.

## References

[1] Andronov, I.V. & Belinskii, B.P., 1995. Scattering of a flexural wave by a finite straight crack in an elastic plate. *J. Sound Vib.* **180**(1), 1–16.

[2] Balmforth, N.J. & Craster, R.V., 1999, Ocean waves and ice sheets. *J. Fluid Mech.* **395**, 89–124.

[3] Belinskiy, B.P., 1982. Optical theorem for the scattering of waves in an elastic plate. *J. Soviet Math.* **20**(1), 1758–1760.

[4] Belinskiy, B.P. & Kouzov, D.P., 1980. Optical theorem for a plate-fluid system. *Soviet Phys. Acoust.* **26**(1), 8–11.

[5] Chung, H. & Fox, C., 2002, Calculation of wave-ice interaction using the Wiener-Hopf technique. *New Zealand J. Math.* **31**(1), 1–18.

[6] Eatock Taylor, R. (Ed.) *The Third International Conference on Hydroelasticity in Marine Technology.* Oxford, UK, September 2003.

[7] Evans, D.V. & Davies, T.V., 1968, Wave-ice interaction. *Report No. 1313, Davidson Lab – Stevens Institute of Technology, New Jersey.*

[8] Evans, D.V. & Porter, R., 2003, Wave scattering by narrow cracks in ice sheets floating on water of finite depth. *J. Fluid Mech.* **484**, 143–165.

[9] Ewing, M. & Crary A.P., 1934, Propagation of elastic waves in ice II. *Physics* **5**, 181–184.

[10] Gradshteyn, I.S. & Ryzhik, I.M., 1981, *Tables of Integrals Series and Products* New York: Academic Press.

[11] Hermans, A.J., 2004, Interaction of free-surface waves with floating flexible strips. *J. Eng. Maths.* **49**, 133–147.

[12] Hertzberg, R., 1996, Deformation and Fracture Mechanics of Engineering Materials. *John Wiley and Sons*, New York.

[13] Norris, A.N. & Wang, Z., 1994, Bending wave diffraction from strips and cracks on thin plates. *Quart. J. Mech. Appl. Math.* **47**(4), 607–627.

[14] Norris, A.N. & Vermula, C., 1995, Scattering of flexural waves on thin plates. *J. Sound Vib.* **181**(1), 115–125.

[15] Porter, R. & Evans, D.V., 2006, Scattering of flexural waves by multiple narrow cracks in ice sheets floating on water. *Wave Motion.* In publication.

[16] Porter, R. & Evans, D.V., 2004. Flexural-gravity wave diffraction by finite cracks of arbitrary shape in ice sheets. *Proc. 19th Int. Workshop on Water Waves and Floating Bodies.* Cortona, Italy.

[17] Robin, G. de Q., 1963, Wave propagation through fields of pack ice. *Phil. Trans. Roy. Soc.* **255** A1057, 313–339.

[18] Squire, V.A. & Dixon A.W., 2000, An analytic model for wave propagation across a crack in an ice sheet. *Int. J. Offshore & Polar Eng.* , **10**, 173–176.

[19] Squire, V.A., Dugan, J.P., Wadhams, P., Rottier, P.J., & Liu, A.K., 1995, Of ocean waves and ice sheets. *Ann. Rev. Fluid Mech.* **27**, 115–168.

[20] Stoker, J.J., 1957, *Water Waves* New York: Wiley-Interscience.

[21] Timoshenko, S & Woinowsky-Krieger, S., 1959, *Theory of Plates and Shells* 2nd Edn. McGraw-Hill.

[22] Tkacheva, L.A., 2001, Surface wave diffraction on a floating elastic plate. *Fluid Dynamics* **36**, 776–789.

[23] Williams, T.D. & Squire, V.A., 2002, Wave propagation across an oblique crack in an ice sheet. *Int. J. Offshore & Polar Eng.* **12**, 157–162.

[24] Williams, T.D. 2005, Reflections on ice: The scattering of flexural-gravity waves by irregularities in arctic and antarctic ice sheets. Ph.D. Thesis, University of Otago, New Zealand.